

https://doi.org/10.1070/QEL17254

Spectroscopic study of $GdVO_4$:Yb + Er crystals

S.A. Klimin, P. Loiseau, D. Caurant, M.N. Popova

Abstract. **$GdVO_4$ crystals doped with different erbium and ytterbium concentrations have been grown in order to study their spectroscopic and kinetic properties and identify the nature of active centres in them. Their polarised transmission and luminescence spectra have been used to construct energy level diagrams of the Er^{3+} ion. The lifetime of the lower level of the $^4I_{11/2}$ excited-state multiplet has been shown to decrease markedly with increasing ytterbium concentration. Inequivalent erbium centres have been observed to form in the crystals with increasing ytterbium concentration.**

Keywords: *$GdVO_4$:Yb + Er, Stark levels, luminescence, lifetime, inequivalent centres.*

1. Introduction

Yb^{3+} and Er^{3+} ions are widely used as a pair in photonics in multilayer film light sources [1], microchip lasers [2], novel compact 'eye-safe' fibre lasers [3], efficient up-conversion sources [4, 5], optical memory [6], etc. The Yb^{3+} and Er^{3+} trivalent ions, a sensitiser and an activator, respectively, serve different functions: owing to its rich system of energy levels, erbium allows one to obtain emission in different spectral ranges, whereas ytterbium ensures strong pump absorption and efficient energy transfer to erbium (Fig. 1). RVO_4 (R = Gd, Y) vanadate crystals (zircon structure) doped with erbium and ytterbium optically active ions have excellent optical characteristics [7–14]. They are commonly known to be promising and widely used laser materials owing to their unique properties: good chemical stability, excellent thermal conductivity and large absorption and emission cross sections [15–19].

Gadolinium vanadate has the zircon ($ZrSiO_4$ mineral) structure. It has the form of colourless crystals with tetragonal symmetry: space group $I4_1/amd$ ($Z = 4$), unit-cell parameters $a = 0.7212$ nm and $c = 0.6346$ nm [20]. Its crystal structure is schematised in Fig. 2. Each gadolinium atom is coordinated by eight O^{2-} oxygen ions. The gadolinium site has point symmetry D_{2d}. The GdO_8 polyhedra form a three-dimensional network. Each polyhedron shares one edge with each of the four adjacent GdO_8 polyhedra. In addition, the GdO_8 polyhedra are linked through VO_4 tetrahedra isolated from each other.

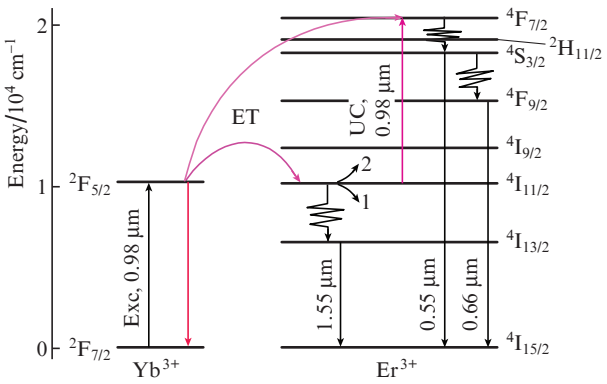

Figure 1. Energy level diagram of the Yb^{3+} and Er^{3+} ions, showing multiplets and the wavelengths of some transitions; Exc, excitation; ET, energy transfer; process 1: nonradiative relaxation and emission; process 2: up-conversion (UC).

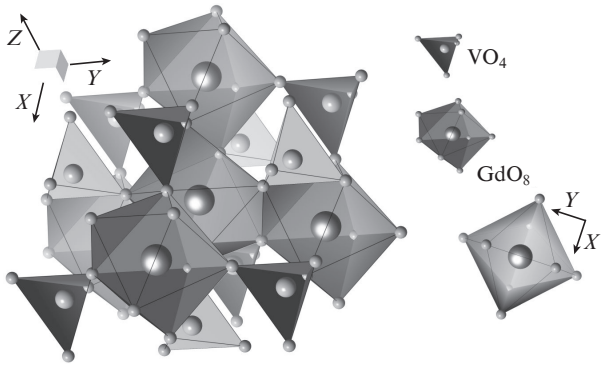

Figure 2. Partial crystal structure of $GdVO_4$. Right side: GdO_8 polyhedron projected along the twofold rotation axis parallel to the crystallographic axis Z.

The Er^{3+} ion has a rich set of optical transitions, among which the $^4I_{13/2} \rightarrow {}^4I_{15/2}$ transition falls in the very important spectral range around $\lambda = 1.5$ μm. This spectral range is of great interest for telecommunications because here silica fibre has a minimum absorption. Besides, the spectral range 1.5–1.6 μm is known to be eye-safe and is used in telemetry. The ability to improve the performance of emitters operating in this range, including laser sources, has been the subject of

S.A. Klimin, M.N. Popova Institute for Spectroscopy, Russian Academy of Sciences, Fizicheskaya ul. 5, Troitsk, 108840 Moscow, Russia; e-mail: klimin@isan.troitsk.ru;
P. Loiseau, D. Caurant Chimie ParisTech, PSL Research University, CNRS, Institut de Recherche de Chimie Paris, 75005, Paris, France

Received 4 February 2020
Kvantovaya Elektronika **50** (3) 259–262 (2020)
Translated by O.M. Tsarev

extensive studies (see e.g. Refs [21–24]). In the Er–Yb codoped samples, process 1 (Fig. 1: relaxation from the $^4I_{11/2}$ multiplet to $^4I_{13/2}$, followed by emission at $\lambda = 1.55$ μm) competes with process 2 – up-conversion through energy transfer from ytterbium to excited erbium, which is thus brought to the $^4F_{7/2}$ state, following which visible emission channels appear. In practice, processes 1 [3, 12] and 2 [7, 8, 10, 11, 14, 16] occur simultaneously.

Despite the extensive studies of the optical properties of erbium- and/or ytterbium-doped $GdVO_4$ crystals and nanopowders, information about the energy level structure of Er^{3+} and Yb^{3+} ions in this host is still limited. In this paper, we report a systematic study of the energy level structure of optically active erbium and ytterbium ions in $GdVO_4$ crystals. $GdVO_4$ single crystals doped with different erbium and ytterbium concentrations were grown by the Czochralski technique. Their spectroscopic properties were studied by optical absorption and luminescence spectroscopies. We determined the lifetime of the Er^{3+} $^4I_{11/2}$ level in different crystals and examined how it was influenced by the sensitiser concentration.

2. Experimental

We grew $GdVO_4$:Er (1 at %), $GdVO_4$:Yb (2 at %), $GdVO_4$:Yb (10 at %) + Er (0.5 at %) and $GdVO_4$:Yb (37 at %) + Er (0.5 at %) single crystals. For measurements, we prepared plane-parallel plates whose faces were parallel to the c axis. Transmission spectra were obtained at temperatures from 4.5 to 300 K and frequencies from 5 000 to 22 500 cm^{-1} on a Bruker IFS 125HR high-resolution Fourier transform spectrometer. To gain information about the symmetry of levels, spectra were measured for two light polarisations: σ ($\boldsymbol{k} \perp c$, $\boldsymbol{E} \perp c$, $\boldsymbol{H} \| c$) and π ($\boldsymbol{k} \perp c$, $\boldsymbol{E} \| c$, $\boldsymbol{H} \perp | c$).

Luminescence spectra were excited by the radiation from an argon laser (Coherent Innova 90) pumped Ti:sapphire laser (Coherent Ring Model 899) and synchronously detected using a monochromator fitted with a PbS detector. In lifetime measurements, excitation was provided by a parametric oscillator at the absorption wavelength of the Yb^{3+} ion. The oscillator was pumped by the BMI Nd:YAG third harmonic. The excitation pulse duration was 10 ns. The emission from the sample was detected at the monochromator output using an InGaAs detector and 150-MHz digital oscilloscope. The signal was averaged over 256 measurements.

3. Results and discussion

In the crystal structure of $GdVO_4$, the Gd^{3+} trivalent ions and rare-earth (RE) substituents occupy sites of tetragonal symmetry (point group D_{2d}). The wave functions of an RE ion having an odd number of electrons (as in Er^{3+} and Yb^{3+}) transform according to the Γ_6 and Γ_7 irreducible representations of point group D_{2d}. Table 1 presents nonzero components of the electric and magnetic dipole moments for optical transitions in this symmetry group. It is seen that the $\Gamma_7 \leftrightarrow \Gamma_6$ electric dipole (ED) transitions are allowed for both the σ- and π-polarisations. At the same time, the $\Gamma_7 \rightarrow \Gamma_7$ and $\Gamma_6 \rightarrow \Gamma_6$ ED transitions can only be observed in the case of σ-polarisation.

Figure 3 shows transmission spectra of the $GdVO_4$:Er (1 at %) crystal in the spectral range of the Er^{3+} $^4I_{15/2} \rightarrow {}^4I_{11/2}$ intermultiplet transition for both σ- and π-polarisations. This multiplet consists of six doublets, three of each symmetry: $3\Gamma_6 + 3\Gamma_7$. We assume the ground state of the Er^{3+} ion to have Γ_7 symmetry, as in YVO_4:Er [25] and the isostructural compound YPO_4:Er [26]. Since the energy of the first excited state of the Er^{3+} ion in the crystal under study is 39 cm^{-1}, as evaluated from spectra, only the ground state is populated at a temperature of 4.5 K, so just six lines, corresponding to transitions from the ground state (of Γ_7 symmetry) to the six levels of the $^4I_{15/2} \rightarrow {}^4I_{11/2}$ multiplet, should be seen in the spectrum of the $^4I_{11/2}$ transition. According to selection rules, three lines of $\Gamma_7 \rightarrow \Gamma_6$ ED transitions are allowed for π-polarisation, which we observe as strong lines in Fig. 3b. The $\Gamma_7 \rightarrow \Gamma_7$ transitions for π-polarisation can show up only as MD transitions. In the case of σ-polarisation, all transitions are allowed in the ED approximation. Thus, we were able to determine not only the energy but also the symmetry of the Stark levels of the $^4I_{11/2}$ multiplet (Table 2). Also indicated in Table 2 are the present data for the $^4I_{13/2}$ multiplet. The energies of the $^4I_{13/2}$ multiplet levels determined in this study agree well with those reported by Ter-Gabrielyan et al. [12].

Table 1. Nonzero components of the electric and magnetic dipole moments, d_i and μ_i ($i = x, y, z$), respectively, of transitions for point group D_{2d} and ions having an odd number of electrons. The subscripts e (electric dipole, ED) and m (magnetic dipole, MD) indicate allowed transitions for the corresponding polarisation.

D_{2d}	Γ_6	Γ_7
	d_x, d_y	d_z, d_x, d_y
Γ_6	μ_z, μ_x, μ_y	μ_x, μ_y
	$(\sigma_{e,m}, \pi_m)$	$(\sigma_e, \pi_{e,m})$
	d_z, d_x, d_y	d_x, d_y
Γ_7	μ_x, μ_y	μ_z, μ_x, μ_y
	$(\sigma_e, \pi_{e,m})$	$(\sigma_{e,m}, \pi_m)$

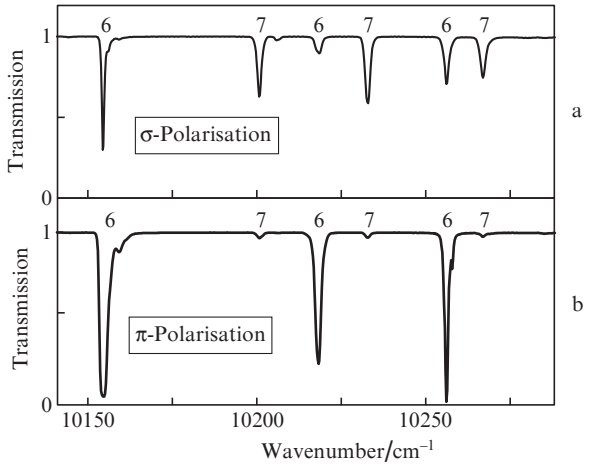

Figure 3. Transmission spectra of the $GdVO_4$:Er (1 at %) sample for the Er^{3+} $^4I_{15/2} \rightarrow {}^4I_{11/2}$ transition at a temperature of 4.5 K in polarised light for (a) σ- and (b) π-polarisations. Also indicated are representations of the symmetry group D_{2d}: 6 (Γ_6) and 7 (Γ_7) of the $^4I_{11/2}$ multiplet levels.

Figure 4 shows absorption spectra of the $GdVO_4$:Er (1 at %), $GdVO_4$:Yb (2 at %) and $GdVO_4$:Yb (10 at %) + Er (0.5 at %) crystals. It is seen that the Er^{3+} and Yb^{3+} ions in the $GdVO_4$ host have identical lower level energies of the $^4I_{11/2}$(Er) and $^2F_{5/2}$(Yb) multiplets, which is a critical condition for efficient energy transfer. The lines at 10155 cm^{-1} in

Table 2. Energies (E) and symmetries of the Stark levels of the $^4I_{13/2}$ and $^4I_{11/2}$ multiplets.

$^4I_{13/2}$		$^4I_{11/2}$	
E/cm^{-1}	Symmetry	E/cm^{-1}	Symmetry
6536.9 (6539)	7	10155	6
6537.9 (6549)	6	10200	7
6578.9 (6581)	7	10218	6
6588.9 (6591)	7	10233	7
6628.2 (6630)	6	10256	6
6679.3 (6681)	6	10267	7
6697.4 (6698)	7		

Note. The numbers in brackets are data from Ref. [12].

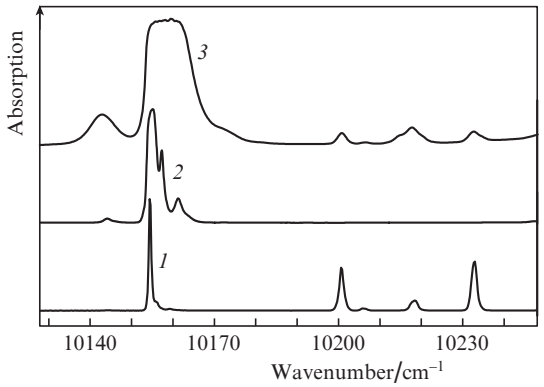

Figure 4. Absorption spectra of the (*1*) $GdVO_4$:Er (1 at %), (*2*) $GdVO_4$:Yb (2 at %) and (*3*) $GdVO_4$:Yb (10 at %) + Er (0.5 at %) samples in the region of the Yb^{3+} 0–0 transition at a temperature of 4.5 K.

stpectra *1* and *2* are seen to have weak satellites, which are probably due to RE pair centres [27, 28].

Figure 5a shows luminescence spectra in the region of the $^4I_{13/2} \rightarrow {}^4I_{15/2}$ transition at liquid-nitrogen and room temperatures. At the higher temperature, the emission lines are broad. Cooling markedly reduces their width and leads to an intensity redistribution due to changes in level populations in the upper multiplet, which are determined by the Boltzmann distribution. Analysis of the spectra with the use of the data in Table 2 makes it possible to identify all spectral lines with certainty and reliably determine the energies of the upper Stark levels 6, 7 and 8 of the $^4I_{15/2}$ multiplet in Fig. 5b: 245, 265 and 300 cm^{-1}, respectively. The measured lifetime of the lower level of the $^4I_{11/2}$ multiplet in the $GdVO_4$:Er (1 at %) crystal is 230 μs. In the codoped Yb–Er samples, the fluorescence around 1 μm originates from the thermalised $^2F_{5/2}$(Yb) and $^4I_{11/2}$(Er) multiples and the measured lifetime decreases to 195 μs in the case of $GdVO_4$:Yb (10 at %) + Er (0.5 at %) and is even shorter (79 μs) in the $GdVO_4$:Yb (37 at %) + Er (0.5 at %) crystal. At the same time, the lifetime of the $^4I_{13/2}$ state is essentially independent of the ytterbium concentration in the crystals: ~2.76 ms. The decrease in the lifetime of the $^4I_{11/2}$ state with increasing ytterbium concentration is likely due to the increase in up-conversion probability (Fig. 1, process 2).

Figure 6 shows the line shapes in the low-temperature transmission spectra for the same transitions in two $GdVO_4$ crystals: one singly doped with erbium and the other codoped with erbium and ytterbium. In the former case, the lines are rather narrow and their width is determined by inhomogeneous broadening. In the latter, each line has a complex shape and is a combination of a few lines. A similar line shape in spectra of RE ions was observed by us previously for other compounds codoped with RE ions [29–31]. It occurs when the nearest neighbour environment of an RE ion contains another RE ion having a different ionic radius. As shown in Fig. 2, each gadolinium ion in $GdVO_4$ has four gadolinium ions as nearest neighbours. The $GdVO_4$:Yb (10 at %) + Er (0.5 at %) crystal can contain different erbium centres: a usual centre, surrounded by four gadolinium ions; a centre in which one nearest neighbour site is occupied by ytterbium instead of gadolinium; etc. Thus, there are inequivalent centres. Since the Gd^{3+} and Yb^{3+} ions differ in ionic radius, the GdO_8 and YbO_8 polyhedra are distorted because they share

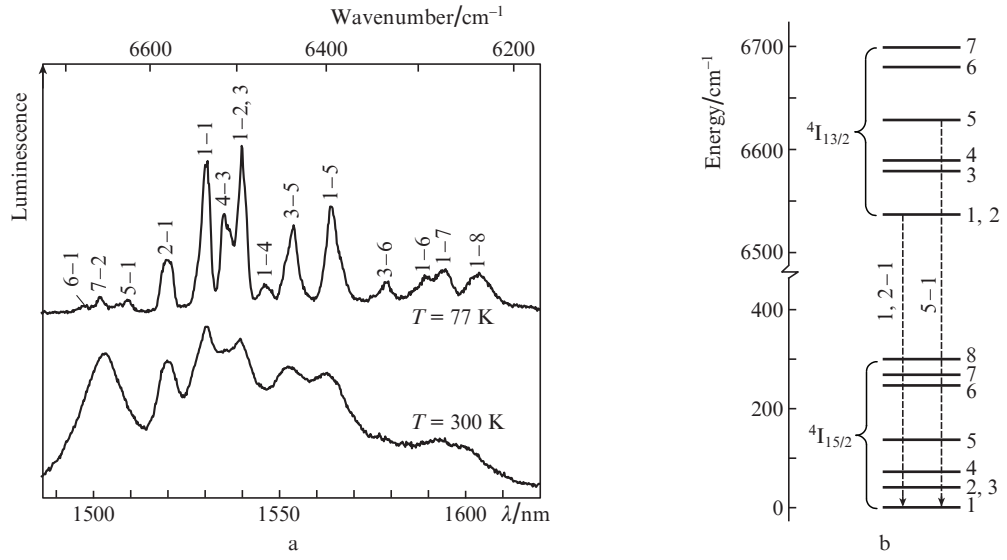

Figure 5. (a) Luminescence spectra of the $GdVO_4$:Yb (37 at %) + Er (0.5 at %) crystals at temperatures of 77 and 300 K; (b) energy level diagram of the $^4I_{15/2}$ ground-state and $^4I_{13/2}$ excited-state multiplets, with some spectral transitions indicated.

one edge, or in other words two oxygens. The crystal field distortion for such a centre entails corrections to its Hamiltonian and, accordingly, corrections to its Stark level energies. As shown earlier [30, 31], the integrated intensities of envelopes constituting a composite line are proportional to the probabilities (P) of formation of inequivalent centres. Such probability can be found as

$$P = C_n^4 x^4 (1 - x)^{4-n}, \quad (1)$$

where x is the fraction of an impurity ion producing defects and n is the number of nearest neighbour impurity atoms. The situation can also be described in terms of clusters. The main cluster has the form of $ErGd_4$; a centre with one defect is an $ErYbGd_3$ cluster. Using relation (1), it is easy to obtain that, in the case of $GdVO_4$:Yb (10 at %) + Er (0.5 at %), the probability of formation of the main cluster is ~0.65 and that of the first defect cluster is 0.29. At first glance, such relations qualitatively describe the complex line shapes in the spectra in Fig. 6.

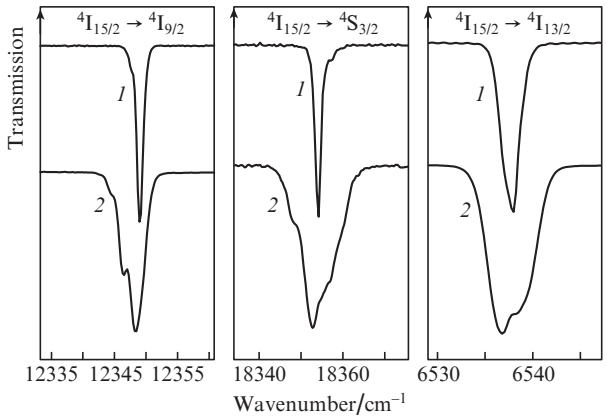

Figure 6. Spectral lines of the $^4I_{15/2} \rightarrow {}^4I_{9/2}$, $^4I_{15/2} \rightarrow {}^4S_{3/2}$ and $^4I_{15/2} \rightarrow {}^4I_{13/2}$ transitions for the (*1*) $GdVO_4$:Er (1 at %) and (*2*) $GdVO_4$:Yb (10 at %) + Er (0.5 at %) samples at a temperature of 4.5 K, demonstrating the presence of inequivalent centres in the ytterbium-rich sample.

4. Conclusions

Polarised transmission spectra of erbium- and ytterbium-doped $GdVO_4$ crystals have been measured for the first time, and information about the energies and symmetries of the Stark levels of the $^4I_{11/2}$ and $^4I_{13/2}$ multiplets has been obtained. Varying the ytterbium doping level (ytterbium concentration) changes the probabilities of phonon relaxation and up-conversion from the $^4I_{11/2}$ multiplet. The formation of inequivalent erbium centres with increasing ytterbium concentration leads to complex, multicomponent shapes of the spectral lines corresponding to Er^{3+} intermultiplet transitions.

Acknowledgements. This work was supported through the Photonic Technologies in Probing Inhomogeneous Media and Biological Objects Program.

References

1. Bai G., Yang Z., Lin H., Jie W., Hao J. *Nanoscale*, **10**, 9261 (2018).
2. Du T., Luo Z., Yang R., Huang Y., et al. *Opt. Lett*., **42**, 462 (2017).
3. Galagan B.I., Denker B.I., Egorova O.N., Kamynin V.A., Ponosova A.A., Sverchkov S.E., Semjonov S.L., Tsvetkov V.B. *Quantum Electron*., **48**, 550 (2018) [*Kvantovaya Elektron*., **48**, 550 (2018)].
4. Du K., Xu X., Yao S., Lei P., Dong L., Zhang M., Feng J., Zhang H. *CrystEngComm*, **40**, 1945 (2018).
5. Zhang Q., Yue S., Sun H., Wang X., Hao X., An S. *Mater. Chem. C*, **5**, 3838 (2017).
6. Wolter B., Pullen M.G., Baudisch M., Sclafani M., Hemmer M., Senftleben A., Schröter C.D., et al. *Phys. Rev. X*, **5**, 021034 (2015).
7. Min B.H., Jung K.Y. *RSC Adv*., **9**, 20002 (2019).
8. Gavrilović T.V., Jovanović D.J., Lojpur V., Dramiéanin M.D. *Sci. Sintering*, **47**, 221 (2015).
9. Gavrilović T.V., Jovanović D.J., Lojpur V., Nikolić A., Dramiéanin M.D. *Sci. Rep*., **4**, 4209 (2014).
10. Khrushchalina S.A., Ryabochkina P.A., Kyashkin V.M., Vanetsev A.S., Gaitko O.M., Tabachkova N.Yu. *JETP Lett*., **103**, 302 (2016) [*Pis'ma Zh. Eksp. Teor. Fiz*., **103**, 342 (2016)].
11. Petrov V.V., Pestryakov E.V., Trunov V.I., et al. *Proc. SPIE*, **6731**, 67310I (2007).
12. Ter-Gabrielyan N., Fromzel V., Ryba-Romanowski W., Lukasiewicz T., Dubinskii M. *Opt. Express*, **20**, 6080 (2012).
13. Savchuk O.A., Carvajal J.J., Cascales C., Aguiló M., Díaz F. *ACS Appl. Mater. Interfaces*, **8**, 7266 (2016).
14. Mahata M.K., Tiwari S.P., Mukherjee S., Kumar K., Rai V.K. *J. Opt. Soc. Am. B*, **31** (8), 1814 (2014).
15. Sokolska I., Heumann E., Kiick S., et al. *Adv. Solid-State Lasers*, **50**, 378 (2001).
16. Zhuang N.F., Hu X.L., et al. *Appl. Phys. B*, **82**, 607 (2006).
17. Dimitrov D., Rafailov P., Marinova V., et al. *J. Phys. Conf. Ser*., **794**, 012029 (2017).
18. Huber G., Kränkel C., Petermann C. *J. Opt. Soc. Am. B*, **27**, B93 (2010).
19. Gorbachenya K.N., Kisel' V.E., Yasyukevich A.S., Matrosov V.N., Tolstik N.A., Kuleshov N.V. *J. Appl. Spectrosc*., **82**, 208 (2015) [*Zh. Prikl. Spektrosk*., **82**, 2214 (2015)].
20. Mullica D.F., Sappenfield E.L., Abraham A.A., Chakoumakos B.C., Boatner L.A. *Inorg. Chim. Acta*, **248**, 88 (1996).
21. Trikshev A.I., Kamynin V.A., Tsvetkov V.B., Itrin P.A. *Quantum Electron*., **48**, 1109 (2018) [*Kvantovaya Elektron*., **48**, 1109 (2018)].
22. Gorlachuk P.V., Ivanov A.V., Kurnosov V.D., Kurnosov K.V., Marmalyuk A.A., Romantsevich V.I., Simakov V.A., Chernov R.V. *Quantum Electron*., **48**, 495 (2018) [*Kvantovaya Elektron*., **48**, 495 (2018)].
23. Dyudelev V.V., Mikhailov D.A., Andreev A.D., et al. *Quantum Electron*., **49**, 1158 (2019) [*Kvantovaya Elektron*., **49**, 1158 (2019)].
24. Ponosova A.A., Azanova I.S., Mironov N.K., Yashkov M.V., Riumkin K.E., Kel' O.L., Sharonova Yu.O., Melkumov M.A. *Quantum Electron*., **49**, 693 (2019) [*Kvantovaya Elektron*., **49**, 693 (2019)].
25. Capobianco J.A., Kabro P., Ermeneux F.S., Moncorge R., Bettinelli M., Cavalli E. *Chem. Phys*., **214**, 329 (1997).
26. Popova M.N., Klimin S.A., Moiseev S.A., Gerasimov K.I., Minnegaliev M.M., Baibekov E.I., Shakurov G.S., Bettinelli M., Chou M.C. *Phys. Rev. B*, **99**, 235151 (2019).
27. Pytalev D.S., Klimin S.A., Popova M.N. *Phys. Lett. A*, **372**, 3506 (2008).
28. Pytalev D.S., Klimin S.A., Popova M.N. *Phys. Lett., A*, **372**, 2332 (2008).
29. Sattayaporn S., Loiseau P., Aka G., Klimin S., Boldyrev K., Mavrin B. *J. Lumin*., **219**, 116895 (2020).
30. Popova M.N., Klimin S.A., Higel P., Dhalenne G. *Phys. Lett. A*, **354**, 487 (2006).
31. Narozhnyy M.V., Klimin S.A., Popova E.A., Dhalenne G. *J. Rare Earths*, **27**, 603 (2009).